2014 International Conference on Unmanned Aircraft Systems (ICUAS)
May 27-30, 2014. Orlando, FL, USA

Nonlinear Model Predictive Control for a multi-rotor with heavy slung load

Jan Trachte
Institute of Flight Mechanics and Control
Universität Stuttgart
70569 Stuttgart, Germany

Felipe Gonzalez
Science and Engineering Faculty
Queensland University of Technology
4001 Brisbane, Australia

Aaron McFadyen
Australian Research Centre for
Aerospace Automation (ARCAA)
4008 Brisbane, Australia

***Abstract*—In this paper a novel controller for stable and precise operation of multi-rotors with heavy slung loads is introduced. First, simplified equations of motions for the multi-rotor and slung load are derived. The model is then used to design a Nonlinear Model Predictive Controller (NMPC) that can manage the highly nonlinear dynamics whilst accounting for system constraints. The controller is shown to simultaneously track specified waypoints whilst actively damping large slung load oscillations. A Linear-quadratic regulator (LQR) controller is also derived, and control performance is compared in simulation. Results show the improved performance of the Nonlinear Model Predictive Control (NMPC) controller over a larger flight envelope, including aggressive maneuvers and large slung load displacements. Computational cost remains relatively small, amenable to practical implementation. Such systems for small Unmanned Aerial Vehicles (UAVs) may provide significant benefit to several applications in agriculture, law enforcement and construction.**

I. Introduction

The utilisation of autonomous Unmanned Aerial System (UAS) is increasing rapidly. They can be a useful tool in civilian applications due to their low cost and availability driven by technological advances. UAS are beginning to emerge in the plant biosecurity sector for a range of applications. Often considered a form of agriculture, plant biosecurity involves the management of invasive pests and diseases for various agricultural and natural assets. Some specific tasks include the precise spatially directed application of concentrated pesticides and close proximity sensing of crop state. While autonomous surveillance, in particular visual pest detection, is already an established key feature in agricultural automation, treating affected areas often involves wide-area spraying of pesticides [1]. A less invasive way to accomplish these tasks is to use small slung load equipped UAS, capable of slow flight. This has the added advantage of positioning the slung load very near or even inside the crop's canopy, allowing precise application of highly concentrated small volume pesticides. As a result, the potential for wind induced dispersal is reduced. Slung load equipped UAS may also help with other sensitive applications, including carriage of precision meteorological instruments, that must be positioned away from the main body of the vehicle.

Conventional control of Unmanned Aerial Vehicle (UAV), in particular multi-rotors, can induce unwanted motion or even become unstable due to heavy slung load. The load impact on the underlying system dynamics should not be neglected as significant feedback forces may be induced on the vehicle during certain flight manoeuvres. The affects of wind and turbulence may be amplified and modified altitude constraints are required to avoid load-ground impact. The constant variation in reference operating point, induced by the slung load, causes conventional controllers to demand increased control effort. Much research has focused on standard multi-rotor position and attitude control [2]–[4] without additional sensor payloads such as a slung load. What remains a challenge is complete control of a slung load system. Some initial work was presented in [5] and [6]. However, predictive control schemes, such as Nonlinear Model Predictive Control (NMPC), have not yet been fully explored and to this end the contributions of this paper are:

1) A novel NMPC for a slung load equipped multi-rotor platform capable of actively damping large load oscillations
2) Quantative performance assessment of NMPC, Model Predictive Control (MPC) and Linear-quadratic regulator (LQR) control for slung load operations in hover, waypoint tracking and aggressive maneuvers
3) Development of a control algorithm that can be easily extended to a real flight environment for field tests

The paper is structured as follows. In section II the nonlinear dynamic system including the slung load is derived. The NMPC is then described in Section III. Preliminary simulation results and a comparative performance assessment is presented in Section IV to VI. Conclusions and further work are outlined in section VII.

II. System Dynamics

The multi-rotor system and the slung load system are derived separately and then coupled by the slung force. The complete system equations are then presented.

A. Multi-Rotor Dynamics

The simplification of the multi-rotor's equations of motion is known to be satisfyingly accurate at low angles [3], [7]. The dynamic model uses the parameters of the X-4 Flyer Mark II, described in "Robotics Toolbox for MATLAB" [8]. The model is used for simulation and validation in section IV and V. Fig. 1 shows the inputs to the multi-rotor; including

978-1-4799-2376-2/14/$31.00 ©2014 IEEE

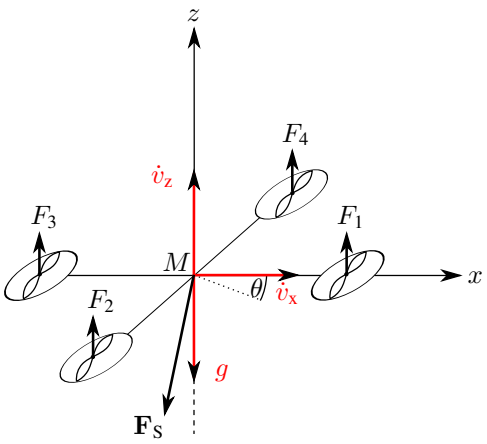

Fig. 1. Simplified multi-rotor dynamics

the pitch angle θ and thrust T controls. The effect of the slung force $\mathbf{F}_S$ on the multi-rotor is also included. However the y-direction is neglected, and the slung load is restricted to move in two dimensions (xz-plane). The resulting accelerations in the inertial system $\dot{v}_x$ and $\dot{v}_z$ are approximated by the following linear equations:

$$\begin{pmatrix} \dot{v}_x \\ \dot{v}_z \end{pmatrix} = \begin{pmatrix} \theta \\ \frac{T}{Mg} - 1 \end{pmatrix} g + \frac{\mathbf{F}_S}{M} \tag{1}$$

where

$$T = \sum_{k=1}^{4} F_k \tag{2}$$

M is the fixed mass of the entire multi-rotor, excluding the load, and g is the gravity constant. The prediction model calculates velocity and position by integration of the corresponding acceleration.

B. Slung Load Dynamics

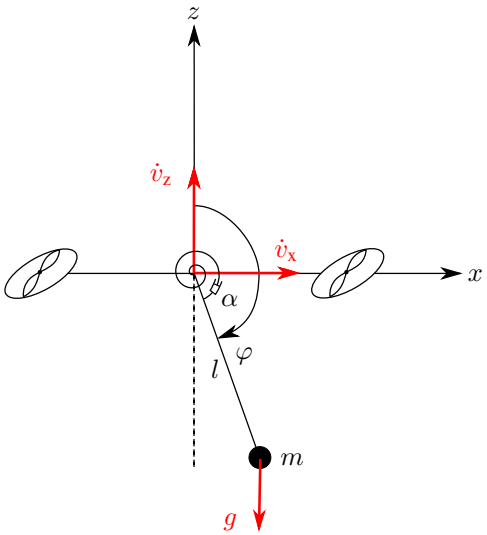

Fig. 2. Simplified 2-d model for slung load force

The derivation of the dynamic equations of the slung load can have several variants, and the complexity increases significantly if the load moves in 3-dimensions or if the slung is considered to become slack during the movement. For this work, the equations of the load are reduced to movement only in the xz-plane. The slung is considered to be rigid and aerodynamic effects on the slung load are neglected. The acting forces are shown in Fig. 2. They include the gravity force g on the load itself and the accelerations $\dot{\mathbf{v}}$ on the pivot, due to the multi-rotor kinematics. The motion is described by

$$\begin{aligned} \dot{\varphi} &= \omega \\ \dot{\omega} &= {}^1\!/\!_l \cdot (g \sin\varphi - \dot{v}_x \cos\varphi + \dot{v}_z \sin\varphi) \underbrace{-\alpha \cdot \omega}_{\text{damping}} \end{aligned} \quad , \tag{3}$$

where φ is the angle to the slung load, ω is the angular speed and α is the damping constant.

The force $\mathbf{F}_S$ is a result of the slung load and consists of the gravitation and centrifugal force. The mass inertia of the load is not considered in the prediction model. It depends on the current angle of the slung load and on the acceleration of the pivot, e.g. the multi-rotor body frame. A simplified equation for the slung force including the slung length l and the load mass m is given by

$$\mathbf{F}_S = (mg\cos\varphi - m\omega^2 l) \begin{pmatrix} \sin\varphi \\ \cos\varphi \end{pmatrix} \quad . \tag{4}$$

C. Integrated Dynamic Model

The following set of equations shows the combined dynamics of the slung load and the multi-rotor. The positions x and z are added to the state vector.

$$\begin{aligned} \begin{pmatrix} \dot{x} \\ \dot{z} \\ \dot{v}_x \\ \dot{v}_z \\ \dot{\varphi} \\ \dot{\omega} \end{pmatrix} &= \begin{pmatrix} 0 & 0 & 1 & 0 & 0 & 0 \\ 0 & 0 & 0 & 1 & 0 & 0 \\ 0 & 0 & 0 & 0 & 0 & 0 \\ 0 & 0 & 0 & 0 & 0 & 0 \\ 0 & 0 & 0 & 0 & 0 & 1 \\ 0 & 0 & 0 & 0 & 0 & -\alpha \end{pmatrix} \begin{pmatrix} x \\ z \\ v_x \\ v_z \\ \varphi \\ \omega \end{pmatrix} \cdots \\ &+ \begin{pmatrix} 0 & 0 \\ 0 & 0 \\ g & 0 \\ 0 & {}^1\!/\!_M \\ 0 & 0 \\ 0 & 0 \end{pmatrix} \begin{pmatrix} \theta \\ T \end{pmatrix} + \begin{pmatrix} 0 \\ 0 \\ {}^m\!/\!_M (g\cos\varphi - \omega^2 l)\sin\varphi \\ {}^m\!/\!_M (g\cos\varphi - \omega^2 l)\cos\varphi - g \\ 0 \\ l(g\sin\varphi - \dot{v}_x\cos\varphi + \dot{v}_z\sin\varphi) \end{pmatrix} \end{aligned} \tag{5}$$

III. Nonlinear Model Predictive Control

The principle of Model Predictive Control (MPC) is to repeatedly solve an open-loop Optimal Control Problem (OCP) at each control step over a finite time horizon [4], [9]. A quadratic cost function J_N is minimized to find the optimal control inputs $\hat{\mathbf{u}}$ subject to the system model $\mathbf{f}(\mathbf{x}, \mathbf{u})$. However, only the first input of the control sequence $\hat{\mathbf{u}}$ is applied, as a new optimal control sequence is calculated at each timestep k. The vector $\mathbf{x} = \begin{bmatrix} x & z & v_x & v_z & \varphi & \omega \end{bmatrix}$ denotes the unconstrained states of the system and the vector $\mathbf{u} = \begin{bmatrix} \theta_{mpc} & T_{mpc} \end{bmatrix}$ denotes the system inputs. θ_{mpc} and T_{mpc} are the desired control inputs and the output of the

MPC. The desired controls θ_{mpc} and T_{mpc} equal the actual states θ and T in the system dynamics of the prediction model. The input constraints are given by

$$\mathbf{u} \in \mathbb{U} \subset \mathbb{R}^2, \quad \mathbb{U} \in [\mathbf{u}_{\min}, \mathbf{u}_{\max}] \tag{6}$$

The optimal control problem can be formally stated as

$$\begin{aligned} \hat{J}_N(\mathbf{x}, \mathbf{u}) = \min \frac{1}{2}(\mathbf{x}_N - \mathbf{x}_N^*)^T P(\mathbf{x}_N - \mathbf{x}_N^*) \\ + \frac{1}{2}\sum_{k=0}^{N-1}(\mathbf{x}_k - \mathbf{x}_k^*)^T Q(\mathbf{x}_k - \mathbf{x}_k^*) \\ + (\mathbf{u}_k - \mathbf{u}_k^*)^T R(\mathbf{u}_k - \mathbf{u}_k^*) \end{aligned} \tag{7}$$

$$\begin{aligned} \text{s.t.} \quad \mathbf{x}_{k+1} = \mathbf{f}(\mathbf{x}_k, \mathbf{u}_k), \quad \forall k = 0, \ldots, N-1 \\ u_k \in \mathbb{U}, \quad \forall k = 0, \ldots, N-1 \end{aligned}$$

where an asterisks $(*)$ denote a reference value and the weighting matrices Q and R are used to penalise deviation from reference states and controls respectively. The terminal penalty matrix P penalises states at the end of the prediction horizon T_p where N is the number of prediction steps. In this paper, $P = Q$. Active set, Sequential Quadratic Programming (SQP) and interior point are all valid solution methods. Active set has shown fast online implementation [10] and is used in this work.

IV. Simulation Framework

A simulation environment was developed using MATLAB and SIMULINK [11]. The predictive control algorithm is implemented by building an interface to the ACADO toolkit [12], which also provides a code generation function to facilitate implementation to a real flight environment. ACADO provides a comprehensive code library that links to the qpOASES [13] solver which applies the active set strategy, that solves the sequential, quadratic subproblems arising from the SQP method. SQP is a well-established numerical method for rapidly solving OCP and NMPC problems [14]. The "Robotics toolbox for MATLAB" [8] is used in the framework as it provides a comprehensive simulation environment, including a 3-dimensional visualization tool. The multi-rotor dynamics are complemented by the slung load's kinematics in the plot function to visualise the movement of the slung load. The feedback force of the swinging load to the multi-rotor is also included. Aerodynamic forces on the load are neglected due to low speeds and a reasonably small drag-coefficient ($c_d \leq 0.5$) of the load is assumed. A low-level Proportional-Integral-Derivative (PID) controller was implemented to regulate the desired multi-rotor pitch angle commanded by the MPC. The PID output provides the individual motor-speeds and is defined in the Laplace domain by

$$u_\theta = \left(K_P + K_I\frac{1}{s} + K_D\frac{K_N}{1 + {}^{K_N}/_s}\right)\Delta\theta \quad , \tag{8}$$

with the error

$$\Delta\theta = \theta_{mpc} - \theta$$

and the parameters $K_P = -8800$, $K_I = -1467$, $K_D = -880$, $K_N = 100$. θ_{mpc} denotes the desired pitch and θ is the current pitch angle. u_θ is the control input, which in this case, is the front and rear motor-speed deflection causing a pitch momentum on the vehicle. The PID gain values (K_P, K_I, K_D, K_N) were selected based on experience and empirical data to resemble standard low-level control of the X-4 Flyer Mark II [15]. The thrust command T_{mpc} is fed forward with a fixed gain K_T to provide the motor-speed deflection $u_T = K_T \cdot T_{mpc}$.

Even though the simulation does not reproduce the exact flight characteristics of the UAV, it is considered to be adequate [15] to validate the implementation as a first approach before migrating to a real-flight environment. A flow chart of the simulation framework is shown in Fig. 3.

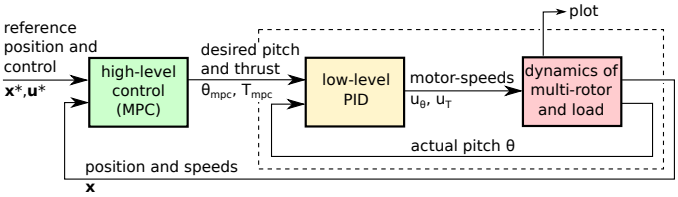

Fig. 3. Simulation Framework

Table I shows the fixed parameters for all simulations. They are derived from the original values of the X-4 Flyer Mark II [15] or augmented to match the conditions of a real flight environment. The upper thrust limit of the original quad-rotor is specified with 130 % of the stationary hover thrust. The 30 % control margin is doubled to ensure maneuverability with an additional heavy swing load, whilst maintaining realistic performance assumptions. A lower limit on thrust is defined to prevent the quad-rotor from descending rapidly or adopting zero thrust. The maximum pitch angle of $\pm 45°$ is set to allow aggressive flight manoeuvres and avoid aerobatic maneuvers where instability is most likely to occur.

V. Results

Three different controllers are designed and three test scenarios are examined for each. These include a MPC without the dynamics of the slung load, the NMPC including the non-linear slung load equations and a LQR. The full non-linear prediction model is linearised about hover and used to derive the linear state space model for the LQR. The same parameters, including the positive definite weighting matrices Q, R, P according Table I were used for all controllers. Three different scenarios were used to evaluate each control technique:

1) **Disturbance Rejection**, where disturbance forces are acting on the UAV whilst attempting to maintain position.
2) **Response to a discontinuous step** of the reference x-position, transitioning from forward flight to hover or vice versa.
3) **Active damping** of a large displacement to the slung load while maintaining position.

The following subsections show plots to visualize the performance of the different control algorithms in the three

TABLE I
SIMULATION PARAMETERS

Name	Symbol	Value
Gravity Constant	g	$9.81\,\mathrm{m\,s^{-2}}$
Mass Multi-rotor	M	$4.0\,\mathrm{kg}$
Mass Slung Load	m	$1.0\,\mathrm{kg}$
Slung Length	l	$1.5\,\mathrm{m}$
Damping Coefficient	α	$0.1\,\mathrm{s^{-1}}$
Simulation time	t_s	$30.0\,\mathrm{s}$
Prediction horizon	T_P	$5.0\,\mathrm{s}$
Prediction steps	N	15
Prediction step size	δ	$1/3\,\mathrm{s}$
Upper limit for inputs	$\mathbf{u}_\mathrm{max}$	$\begin{pmatrix} \pi/4 \\ (1+60\%)Mg \end{pmatrix}$
Lower limit for inputs	$\mathbf{u}_\mathrm{min}$	$\begin{pmatrix} -\pi/4 \\ (1-60\%)Mg \end{pmatrix}$
State weighting matrix (x, z, v_x, v_x, φ, ω)	$\mathbf{Q}$	$\begin{pmatrix} 10 & 0 & 0 & 0 & 0 & 0 \\ 0 & 10 & 0 & 0 & 0 & 0 \\ 0 & 0 & 10^{-9} & 0 & 0 & 0 \\ 0 & 0 & 0 & 10^{-9} & 0 & 0 \\ 0 & 0 & 0 & 0 & 25 & 0 \\ 0 & 0 & 0 & 0 & 0 & 10^{-9} \end{pmatrix}$
Control weighting matrix (θ, F)	$\mathbf{R}$	$\begin{pmatrix} 1 & 0 \\ 0 & 0.1 \end{pmatrix}$
Gain matrix (LQR)	$\mathbf{K}$	$\begin{pmatrix} 3.2 & \sim 0 & 2.2 & \sim 0 & 4.5 & -0.5 \\ \sim 0 & 3.2 \cdot 10^6 & \sim 0 & 5000 & \sim 0 & \sim 0 \end{pmatrix}$

scenarios. The plots only show the first 6 s of the entire simulation since this is sufficient to evaluate the controllers and offers better clarity in the result presentation. Table II-IV also only include values for the first 6 s for consistency.

A. Disturbance Rejection

Disturbance forces act on the body frame of the multi-rotor (F_x, F_z) as well as a torque (T_φ) on the slung load. The characteristics of the disturbances correlate to a constant wind that is combined with a strong wind gust at 1 s of simulation time as shown in Fig. 4. Fig. 5 shows the response of each of the three control algorithms.

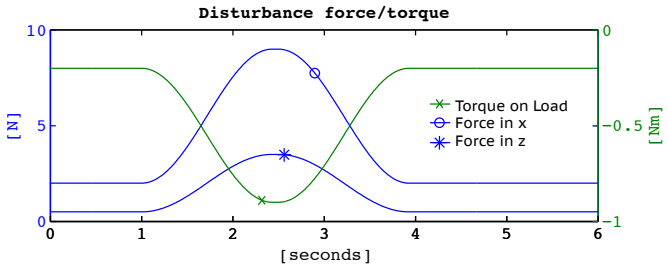

Fig. 4. Forces F_x and F_z on the body frame and a torque T_φ on the slung load

Table II shows the Root Mean Square (RMS) for the plotted x-position, slung load angle and pitch command compared to the reference value. The Control Effort (CE) is derived by an integration of the pitch control θ over the time t. The Control Effort for the NMPC is more than the other controllers and so is the displacement of the slung load from the reference. Also the deviation to the x-reference is higher.

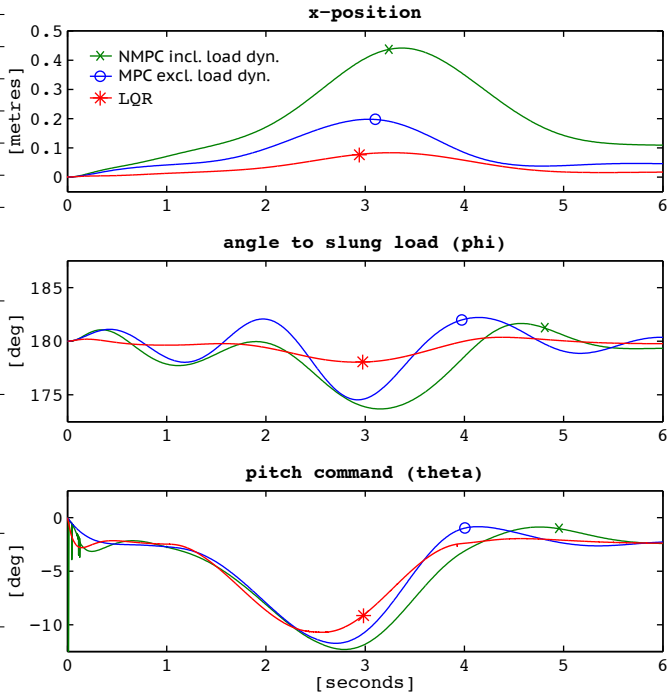

Fig. 5. Disturbance rejection to forces F_x and F_z on the body frame and a torque T_φ on the slung load

TABLE II
RMS AND CONTROL EFFORT FOR DISTURBANCE REJECTION

	RMS x [m]	RMS φ [°]	RMS θ [°]	CE $\int \theta \cdot dt$
NMPC	0.23	178.6	6.0	29.23
MPC	0.11	179.5	6.0	26.69
LQR	0.04	179.5	5.4	26.73

B. Step Response / Waypoint Approach

Fig. 6 shows the response to a discontinuous step on the x-position reference (dashed line) after 1 s of runtime. This corresponds to a new waypoint command. Results of the entire simulation show a unacceptable displacement of the x-position and an increasing oscillation of the load when the Linear-quadratic regulator (LQR) is used. The two predictive controllers rapidly achieve a stationary stable state, with the NMPC including the load dynamics showing a shorter settling time.

Table III shows the RMS and CE for the different controllers. The calculations of these values exclude the first second, as the step in the x-reference is not given before this time.

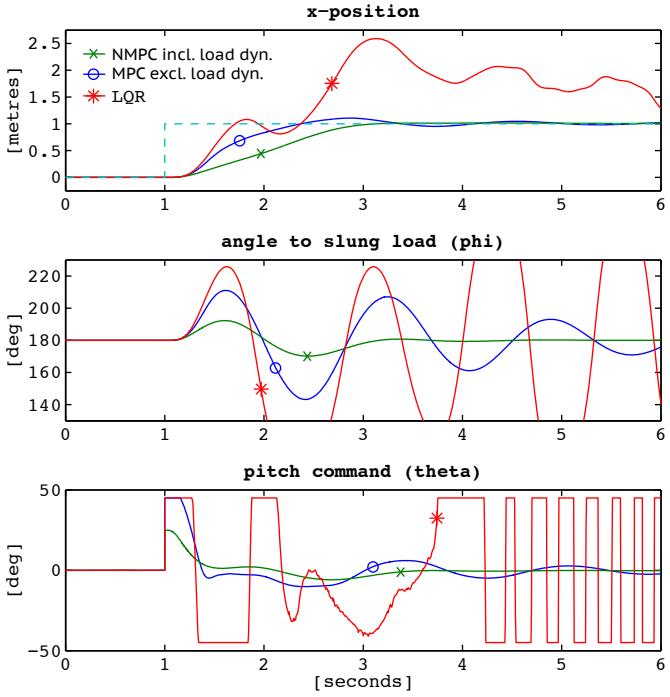

Fig. 6. Response in x-position, pendulum angle and pitch command to a discontinuous step in the reference x-position (dashed line)

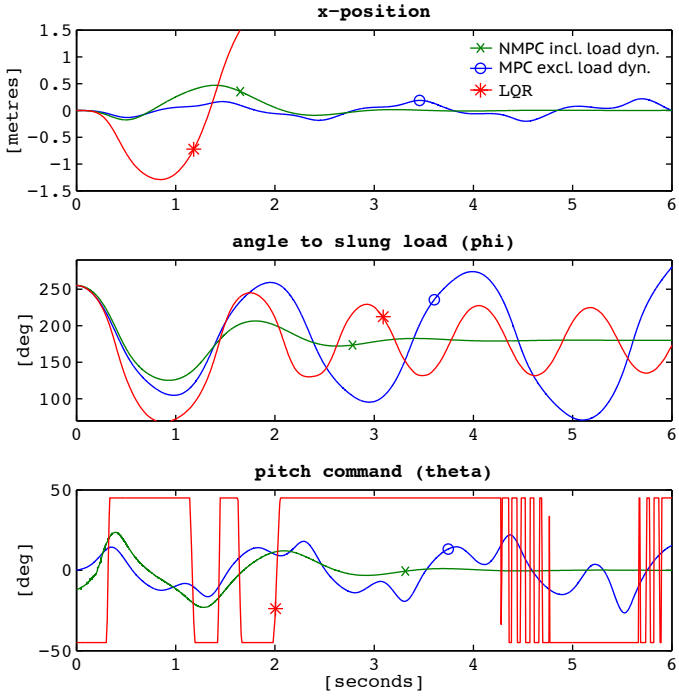

Fig. 7. Slung Load Damping (initial $\Delta\varphi = 75°$)

TABLE III
RMS AND CONTROL EFFORT FOR STEP INPUT

	RMS x [m]	RMS φ [°]	RMS θ [°]	CE $\int \theta \cdot dt$
NMPC	0.57	181.6	11.0	1.70
MPC	0.98	181.7	7.0	4.59
LQR	0.48	180.1	16.5	11.95

C. Slung Load Damping

The ability to actively damp slung load oscillations is studied by offsetting the load to an initial displacement of $\Delta\varphi = 75°$ from the reference equilibrium state. Fig. 7 shows the response of the three control algorithms in x-position, load angular displacement and pitch angle. The LQR becomes unstable very quickly and does not recover to the reference x-position within the simulated time. Although the x-position is maintained, the amplitude of the load oscillations increases constantly for the MPC. This results as the load kinematics are disregarded in the prediction model.

Table IV shows the RMS values and CE for each controller.

TABLE IV
RMS AND CONTROL EFFORT FOR LOAD DAMPING

	RMS x [m]	RMS φ [°]	RMS θ [°]	CE $\int \theta \cdot dt$
NMPC	0.28	180.1	11.6	1.44
MPC	0.12	198.4	12.7	3.54
LQR	2.64	190.4	44.5	69.04

VI. DISCUSSION

The non-linear predictive control (NMPC incl. load dyn.) performs well in all three test cases. The NMPC is not very reactive for the disturbance reaction (subsection V-A) and therefore shows the largest deviation in the x-position with a high RMS, but stays stable for the entire 30 s of simulation-time with reasonable total Control Effort. The LQR performs more accurate in this scenario, with a quick control response and small deviation in x-position and slung load angle. The main reason for this is that the linearisation for the LQR corresponds to the system states at a stable hover. This means good performance for flight attitudes near hover, and poor performance at higher attitude angles, as shown in Fig. 6 and 7. The LQR overshoots and even causes instability. It can be tuned by changing the weighting matrices, which leads to appropriate control commands for particular scenarios. However, this is not considered here to provide comparable results of the different control algorithms. Moreover the weighting matrices of the predictive controllers could be tuned, too. Improvement of the LQR could also be achieved by performing multiple linearisations at different flight attitudes and adaptively adjusting the gain matrices to the corresponding flight attitude. The MPC excluding the load dynamics in the prediction model shows a good performance in maintaining the position, but is not capable of damping the slung load as shown by an increased amplitude of oscillation in Fig. 7. The RMS of the slung load angle therefore shows a high deviation to the reference equilibrium state. This also results in a high control effort as competing objectives, i.e. to maintain position and to reduce oscillation, are not well managed.

VII. Conclusion

The NMPC shows good performance and robustness when non-linearity is significant and varying tasks are given to the controller. The modelling of the slung load is necessary if load swing-damping is required or when the load is heavy (in relation to the multi-rotor) and flying at large attitude. An abrupt emergency stop of a multi-rotor with a slung load is one example where these conditions are met. The NMPC is able to reduce the control effort due to efficient damping of the slung load. Hence, less energy is consumed and the available flight time increases. A LQR is sufficient for small angles near the point of linearisation and provides a simpler and faster solution than the MPC. As expected, the LQR performs badly when high angular displacement of both the vehicle and the slung load occur. Even the linear MPC without the slung load performs better, since it's not limited to the operating point near hover. It is shown that the (N)MPC offers a wider spectrum over the flight envelope of the vehicle with a slung load. However, the simplified prediction model of the multi-rotor cannot account for all conditions. Ongoing work focuses on implementation of non-linear equations of motion, as well as the enhancement of the NMPC to a 3-dimensional, spherical prediction of the slung load. The consideration of aerodynamic forces on the slung load is also been developed in conjunction to an adaptive MPC algorithm that can explicitly manage slackness in the slung load.

Acknowledgment

This work was kindly supported by Queensland University of Technology (QUT), Australian Research Centre for Aerospace Automation (ARCAA) and Plant Biosecurity CRC. The authors would also like to thank to Christoph Seiferth and colleagues at the Institute of Flight Mechanics and Control (IFR) at the University of Stuttgart in Germany.

References

[1] C. Hillnhütter, A. Schweizer, V. Kühnhold, and R. A. Sikora, "Remote sensing for the detection of soil-borne plant parasitic nematodes and fungal pathogens," in *Precision Crop Protection-the Challenge and Use of Heterogeneity*. Springer, 2010, pp. 151–165.

[2] P. Bouffard, "On-board model predictive control of a quadrotor helicopter: Design, implementation, and experiments," 2012.

[3] K. Alexis, G. Nikolakopoulos, and A. Tzes, "Model predictive quadrotor control: attitude, altitude and position experimental studies," *Control Theory and Applications, IET*, vol. 6, no. 12, pp. 1812–1827, 2012.

[4] M. Burri, J. Nikolic, C. Hürzeler, J. Rehder, and R. Siegwart, "Aerial service robots for visual inspection of thermal power plant boiler systems," in *Proc. of the 2nd Int. Conf. on Applied Robotics for the Power Industry*, 2012.

[5] H. M. Omar, "New fuzzy-based anti-swing controller for helicopter slung-load system near hover," in *Computational Intelligence in Robotics and Automation (CIRA), 2009 IEEE International Symposium on*. IEEE, 2009, pp. 474–479.

[6] R. Spica, A. Franchi, G. Oriolo, H. H. Bulthoff, and P. R. Giordano, "Aerial grasping of a moving target with a quadrotor uav," in *Intelligent Robots and Systems (IROS), 2012 IEEE/RSJ International Conference on*. IEEE, 2012, pp. 4985–4992.

[7] A. Mcfadyen, L. Mejias, P. Corke, and C. Pradalier, "Aircraft collision avoidance using spherical visual predictive control and single point features," in *Intelligent Robots and Systems (IROS), 2013 IEEE/RSJ International Conference on*. IEEE, 2013, pp. 50–56.

[8] P. I. Corke, "A robotics toolbox for matlab," *Robotics & Automation Magazine, IEEE*, vol. 3, no. 1, pp. 24–32, 1996.

[9] R. Findeisen and F. Allgöwer, "An introduction to nonlinear model predictive control," in *21st Benelux Meeting on Systems and Control*, vol. 11, 2002.

[10] H. J. Ferreau, H. G. Bock, and M. Diehl, "An online active set strategy to overcome the limitations of explicit mpc," *International Journal of Robust and Nonlinear Control*, vol. 18, no. 8, pp. 816–830, 2008.

[11] (2014). [Online]. Available: http://www.mathworks.com.au/products/simulink/

[12] B. Houska, H. J. Ferreau, and M. Diehl, "Acado toolkit—an open-source framework for automatic control and dynamic optimization," *Optimal Control Applications and Methods*, vol. 32, no. 3, pp. 298–312, 2011.

[13] (2014). [Online]. Available: http://set.kuleuven.be/optec/Software/qpOASES-OPTEC

[14] P. T. Boggs and J. W. Tolle, "Sequential quadratic programming," *Acta numerica*, vol. 4, no. 1, pp. 1–51, 1995.

[15] P. Pounds, R. Mahony, and P. Corke, "Modelling and control of a large quadrotor robot," *Control Engineering Practice*, vol. 18, no. 7, pp. 691–699, 2010.